

High-Pressure XAFS Measurements of the Coordination Environments of Fe²⁺ and Fe³⁺ in Basaltic Glasses

Keisuke Ozawa¹, Kei Hirose², and Yoshio Takahashi³

¹Department of Earth and Planetary Science, The University of Tokyo

²Tokyo Institute of Technology

³The University of Tokyo

November 23, 2022

Abstract

We investigated pressure-induced changes in the coordination environments of Fe²⁺ and Fe³⁺ in basaltic glasses based on the Fe K-edge X-ray absorption fine structure (XAFS) analyses for both XANES and EXAFS regions. Upon compression from 1 bar to ~15 GPa, the Fe²⁺-O bond length remained similar, suggesting that the average coordination number of Fe²⁺ increased from ~5 to 6. On the other hand, the Fe³⁺-O bond was remarkably elongated, which indicates that Fe³⁺ changed from 4-fold to 6-fold coordination. Above 15 GPa, both Fe²⁺-O and Fe³⁺-O bond lengths decreased smoothly, suggesting minor changes in their coordination numbers. The data also showed that both Fe²⁺ and Fe³⁺ remained in the high-spin state up to 83 GPa and 60 GPa, respectively, in the basaltic glasses. These compression behaviors of the Fe²⁺-O and Fe³⁺-O bonds support that Fe²⁺ disproportionates into Fe³⁺ and metal Fe in a deep magma ocean.

High-Pressure XAFS Measurements of the Coordination Environments of Fe²⁺ and Fe³⁺ in Basaltic Glasses

Keisuke Ozawa¹, Kei Hirose^{1,2}, and Yoshio Takahashi^{1,3}

¹Department of Earth and Planetary Science, The University of Tokyo, Tokyo, Japan

²Earth-Life Science Institute, Tokyo Institute of Technology, Tokyo, Japan

³Institute of Materials Structure Science, High-Energy Accelerator Research

Organization, Tsukuba, Ibaraki, Japan

Key Points

- We examined high-pressure coordination environments around Fe²⁺ and Fe³⁺ in basaltic glasses by X-ray absorption spectroscopy to 83 GPa.
- XANES and EXAFS analyses indicate that the coordination numbers of Fe²⁺ and Fe³⁺ increases with increasing pressure from 1 bar to ~15 GPa.
- Compression behaviors of the Fe-O bond lengths support the disproportionation of Fe²⁺ into Fe³⁺ and Fe⁰ in a deep magma ocean.

Abstract We investigated pressure-induced changes in the coordination environments of Fe²⁺ and Fe³⁺ in basaltic glasses based on the Fe K-edge X-ray absorption fine structure (XAFS) analyses for both XANES and EXAFS regions. Upon compression from 1 bar to ~15 GPa, the Fe²⁺-O bond length remained similar, suggesting that the average coordination number of Fe²⁺ increased from ~5 to 6. On the other hand, the Fe³⁺-O bond

was remarkably elongated, which indicates that Fe^{3+} changed from 4-fold to 6-fold coordination. Above 15 GPa, both Fe^{2+} -O and Fe^{3+} -O bond lengths decreased smoothly, suggesting minor changes in their coordination numbers. The data also showed that both Fe^{2+} and Fe^{3+} remained in the high-spin state up to 83 GPa and 60 GPa, respectively, in the basaltic glasses. These compression behaviors of the Fe^{2+} -O and Fe^{3+} -O bonds support that Fe^{2+} disproportionates into Fe^{3+} and metal Fe in a deep magma ocean.

Plain Language Summary The coordination environments around Fe^{2+} and Fe^{3+} in silicates are of great importance for their partial molar volumes, spin states, and partitioning. The local structures around Fe in silicate glasses were intensively studied at 1 bar by XAFS analyses, but their pressure-induced changes have not been examined. Here we conducted the XAFS measurements of Fe^{2+} in a reduced basaltic glass to 83 GPa and Fe^{3+} in an oxidized glass to 60 GPa. While the Fe-O bond is shortened by a simple compression effect, it is elongated due to an increase in the coordination number. The observed changes in the bond length showed that Fe^{2+} was ~5-fold coordinated at 1 bar and became 6-fold with compression to ~15 GPa. On the other hand, the coordination number of Fe^{3+} increased from 4 at ambient pressure to 6 at ~15 GPa. Both were 6-fold coordinated above 15 GPa. These bond lengths also suggest that both Fe^{2+} and Fe^{3+} remained high spin in our measurements. The difference between the Fe^{2+} -O and Fe^{3+} -O bond lengths support a previously-proposed negative volume change upon the disproportionation reaction of Fe^{2+} into Fe^{3+} and Fe^0 above 10 GPa, which enhances such disproportionation in a deep magma ocean.

1. Introduction

Iron is the most abundant transition metal and exhibits multiple oxidation states in the Earth's mantle. The coordination environments and bond lengths of Fe^{2+} -O and Fe^{3+} -O in silicates change with increasing pressure. The spin states of Fe^{2+} and Fe^{3+} could also change not only in solid phases (Badro et al., 2003; Zhang & Oganov, 2006) but also in melts and glasses under high pressure (Nomura et al., 2011; Gu et al., 2012; Karki & Ghosh, 2018). The changes in the Fe^{2+} -O and Fe^{3+} -O bond lengths will tell their possible spin crossovers under lower-mantle pressures. It has been also suggested that Fe^{2+} disproportionates into Fe^{3+} and metal Fe in a deep magma ocean, depending on the partial molar volumes of FeO and $\text{FeO}_{1.5}$ and their compressibilities (O'Neill et al., 2006; Zhang et al., 2017; Armstrong et al., 2019). However, direct measurements of these properties are limited to 1 atm (Lange & Carmichael, 1987; Kress & Carmichael, 1991). They are dependent on the coordination environment of Fe ions, in particular their coordination number and the structure of silicate melts, both of which will change under high pressure (Sanloup et al., 2013a). However, the change in the coordination environment of iron in silicate melt has been experimentally investigated only up to 7.5 GPa by X-ray diffraction measurements (Sanloup et al., 2013b).

The XAFS spectrum is sensitive to the local structure of a specific element of interest including the bond length. It is therefore a useful tool for elucidating changes in the coordination environments and spin states of Fe^{2+} and Fe^{3+} under high pressure. However, the XAFS study of Fe^{2+} and Fe^{3+} in a silicate glass has been difficult at high pressures because diamond anvils absorb X-rays to a large extent at the Fe absorption edge energy (~7.1 keV), while the ambient-pressure XAFS measurements of Fe in silicate glasses have been intensively reported (Farges et al., 2004; Wilke et al., 2007).

Here we conducted the XAFS measurements of Fe^{2+} and Fe^{3+} in reduced and oxidized basaltic glasses, respectively, at high pressures in the fluorescence yield mode (Ozawa et al., 2021). The analyses of X-ray absorption near edge structure (XANES) including pre-edge structure and extended X-ray absorption fine structure (EXAFS) demonstrate changes in the Fe^{2+} -O and Fe^{3+} -O bond lengths with increasing pressure up to 83 GPa and 60 GPa, respectively, indicating their coordination environment and spin state under pressure. Based on these results, we discuss the spin crossover of Fe^{2+} and Fe^{3+} in basaltic glasses and the disproportionation of Fe^{2+} into Fe^{3+} and Fe^0 in a deep magma ocean.

2. Results

We collected nine and eight XAFS (both XANES and EXAFS) spectra of reduced and oxidized basaltic glasses with increasing pressure from 1 bar to 83.2 GPa and to 60.0 GPa, respectively (see Experimental Methods in the Supporting Information). The Fe K-edge XANES spectrum comprises three separate features relating to transitions of electrons to different excited states: pre-edge ($1s \rightarrow 3d$), threshold energy ($1s \rightarrow 4s$), and white line ($1s \rightarrow 4p$) (Waychunas et al., 1983) (Figure 1).

2.1. Pre-edge Structure

The pre-edge features were extracted from the normalized XANES spectra to emphasize their characteristics (Figure 1). The calculated centroid position and integrated intensity for the pre-edge absorbance are given for all the spectra in Table S2. The centroid energy and intensity of the pre-edge absorbance at the Fe K-edge are sensitive to the oxidation state and coordination environment of iron atoms in a sample, respectively (Figure 2).

The centroid position of the reduced basalt glass is 7111.92 eV at ambient pressure (Figure 2), indicating that almost all iron was Fe^{2+} in our reduced glass according to Wilke et al. (2005). Its pre-edge intensity observed at 1 bar is consistent with those for reduced basaltic glasses (Wilke et al., 2005) and reduced silicate melts (Alderman et al., 2017), which shows that the coordination number of Fe^{2+} is close to five. As pressure increased, the pre-edge intensity became closer to those of minerals with octahedrally coordinated ferrous iron (Figure 2). This observation suggests that the average coordination number of Fe^{2+} in our reduced glass increased with compression from ~5 at ambient pressure to 6 above 15 GPa.

On the other hand, the centroid position of the oxidized glass is 7113.40 eV at 1 bar (Figure 2), showing $\text{Fe}^{2+}/\Sigma\text{Fe} = 0.21$, which is consistent with the ratio expected for the condition where this glass was synthesized. Its pre-edge intensity suggests that Fe^{3+} is almost 4-fold at 1 bar. While Wilke et al. (2005) interpreted that Fe^{3+} in their oxidized glass was 5-fold, the pre-edge intensity itself is similar between this study and their measurements, and the discrepancy is attributed to the variation in the pre-edge intensity of reference minerals for tetrahedrally-coordinated Fe^{3+} (Boubnov et al., 2015). The change in the pre-edge intensity with increasing pressure also indicates that the average coordination number of Fe^{3+} increased upon compression from almost 4 at 1 bar to 6 above 15 GPa (Figure 2).

2.2. Absorption Edge Structure

The information on the valence state of Fe ion and the Fe-O bond length are included not only in the pre-edge feature but also in the absorption edge structure, in particular (i) the peak energy of the white line and (ii) the threshold energy, which is a structure around

the maximum of $d\mu_N/dE$ (μ_N , normalized absorbance; E , energy) (Figure 1 and Table S2). It is known that both the white line peak energy and the threshold energy are higher for Fe^{3+} than for Fe^{2+} .

In the case of the reduced glass, the white line peak energy significantly increased with increasing pressure above 15 GPa (Figure 3a). Indeed, the increase in the peak energy is well correlated to the shortening of the average Fe^{2+} -O bond length (see the next section) (Figure S1). Previously Waychunas et al. (1983) reported similar observations in minerals. In contrast, the threshold energy changed little with increasing pressure (Figure 3c). While the first derivative spectrum at ambient pressure had a double-peaked shape (Berry et al., 2003), it gradually became single-peak as pressure increased. The effect of silicate glass composition may be important for the threshold energy; a reduced W-doped basaltic glass exhibited a distinct value (Ozawa et al., 2021) (Figure S2). It contrasts the fact that the compositional effect on the white line peak energy is quite small.

Our data on the oxidized glass demonstrate a negative correlation between the Fe^{3+} -O bond length and the peak position of the white line for Fe^{3+} , similar to the case of Fe^{2+} (Figure S1). The white line peak energy certainly decreased with increasing pressure from 1 bar to ~15 GPa and then increased at higher pressures (Figure 3b). It should be attributed to the increase and subsequent decrease in the Fe^{3+} -O bond length in our oxidized glass (see the next section). The first-derivative spectrum at 1 bar given in Figure 3d is similar to that of an Fe^{3+} -rich silicate glass in Berry et al. (2003). The correlation between the Fe^{3+} -O bond length and the threshold energy is not clear (Figure S2).

2.3. EXAFS Spectra

All of the present XAFS measurements include the EXAFS spectra that provide the Fe-O bond length quantitatively. The extracted k^3 -weighted oscillations are shown in [Figure S3](#). Considering that all Fe was Fe^{2+} in the reduced glass, we determined the Fe^{2+} -O bond length at each pressure from the EXAFS analyses ([Figure 4 and Table S2](#)).

We obtained the Fe^{2+} -O bond length $r_{\text{Fe}^{2+}\text{-O}} = 1.98 \pm 0.02 \text{ \AA}$ at 1 bar for the reduced basaltic glass ([Figure 4a](#)). The $r_{\text{Fe}^{2+}\text{-O}}$ remained constant within errors up to 15.1 GPa, in which the bond length elongation because of an increase in the coordination number was compensated by shortening due to a simple compression effect. At higher pressures, the average Fe^{2+} -O bond length decreased continuously with increasing pressure up to 83.2 GPa. In this pressure range, the effect of the coordination number increase may be minor. The shortening per a given pressure increase above 15 GPa is found to be greater than that of the Si-O (Prescher et al., 2017) and Ge-O bonds (Hong et al., 2014) ([Figure 4b](#)).

The Fe^{3+} -O bond length in our oxidized glass was also determined at each pressure from the EXAFS analyses. At 1 bar, $r_{\text{Fe}^{3+}\text{-O}}$ is found to be $1.87 \pm 0.02 \text{ \AA}$ ([Figure 4a](#)), consistent with the interatomic distance between four-fold Fe^{3+} and O in a peralkaline rhyolitic glass at ambient pressure (Giuli et al., 2012). The Fe^{3+} -O bond length increased with increasing pressure up to 16.2 GPa unlike the case of Fe^{2+} , indicating that the effect of the coordination number increase exceeded the simple bond length shortening by compression. With further compression from 16.2 GPa to 60.0 GPa, the Fe^{3+} -O bond length decreased constantly as for Fe^{2+} .

As described above, we found negative correlations between the Fe^{2+} -O/ Fe^{3+} -O bond lengths and the white line peak energy ([Figure S1](#)), which indicates that the coordination number has little influence on the peak position of the white line. On the other hand, the

threshold energy also shows negative correlation with the Fe^{2+} -O bond length, but does not have a clear correlation with the Fe^{3+} -O bond length (Figure S2). The white line peak position in the XANES spectra can be a good indicator of the Fe^{2+} -O/ Fe^{3+} -O bond lengths in silicate melts and glasses when high-quality EXAFS data are not available.

3. Discussion

3.1. Compression Behaviors of Fe^{2+} and Fe^{3+} in Basaltic Glasses

The present pre-edge and EXAFS analyses showed that Fe^{3+} is almost 4-fold coordinated in our basaltic glass sample at 1 bar, while Fe^{2+} is ~5-fold coordinated (Figure 2). The 4-fold Fe^{3+} is considered to be a network former, polymerizing silicate melt/glass structures and being accompanied with a charge compensator ion like Na^+ and Ca^{2+} . In contrast, the ~5-fold Fe^{2+} is a network modifier or plays an intermediate role (Alderman et al., 2017).

Below ~15 GPa, while the Fe^{2+} -O bond length remained similar, the Fe^{3+} -O bond was elongated remarkably with compression (Figure 4a). Such difference is likely due to the difference in their coordination number at 1 bar; the large increase in the Fe^{3+} -O bond length below 15 GPa is attributed to an increase in the coordination number of ferric iron from four to six, whereas the approximately uniform Fe^{2+} -O bond length is likely a consequence of a small increase in its coordination number from about five to six. At the higher pressure range, both the Fe^{2+} -O and Fe^{3+} -O bond lengths decreased similarly with increasing pressure (Figure 4a), in which the effect of an increase in the coordination number is likely to be minimal.

We compare the pressure-induced changes in the Fe^{2+} -O and Fe^{3+} -O bond lengths observed in this study with those of Mg^{2+} -O (Ghosh & Karki, 2020), Ca^{2+} -O and Al^{3+} -O

(Ghosh & Karki, 2018), $\text{Si}^{4+}\text{-O}$ (Prescher et al., 2017), $\text{Ge}^{4+}\text{-O}$ (Hong et al., 2014), and $\text{W}^{6+}\text{-O}$ (Ozawa et al., 2021) previously reported in silicate/germanate melt and glasses (Figure 4a, b). For both Mg^{2+} and Ca^{2+} , the bond lengths are almost constant from ambient pressure to 15 GPa, similar to the case of $\text{Fe}^{2+}\text{-O}$, indicating that the bond elongation by coordination number increase and the bond shortening by a simple compression effect are balanced. In contrast, the $\text{Al}^{3+}\text{-O}$ bond length increases with pressure to 15 GPa as for Fe^{3+} , which indicates the role of Fe^{3+} in silicate glass structures is similar to that of Al^{3+} at such low pressure range. At higher pressures (>15 GPa for Ca^{2+} , Mg^{2+} , Al^{3+} , Fe^{2+} , and Fe^{3+} , $>\sim 20$ GPa for Ge^{4+} , and $>\sim 30$ GPa for Si^{4+} and W^{6+}), the bond lengths then decrease with compression (Figure 4a, b). The $\text{Fe}^{2+}\text{-O}$ and $\text{Fe}^{3+}\text{-O}$ bond lengths became shorter by -0.0015 \AA/GPa and -0.0017 \AA/GPa , respectively. They are equivalent to -0.0017 \AA/GPa for $\text{Mg}^{2+}\text{-O}$ in $(\text{Mg,Fe})\text{SiO}_3$ melt at 3000 K (Ghosh & Karki, 2020) and -0.0024 \AA/GPa for $\text{Ca}^{2+}\text{-O}$ in $\text{CaAl}_2\text{Si}_2\text{O}_8$ glass (Ghosh & Karki, 2018). The similarity to the $\text{Mg}^{2+}\text{-O}$ and $\text{Ca}^{2+}\text{-O}$ bonds suggests that not only Fe^{2+} but also Fe^{3+} act as network modifiers under high pressures where they are predominantly six-fold coordinated. In contrast, for high field strength elements (with large valence/ionic-radius ratios), $\text{Si}^{4+}\text{-O}$ in SiO_2 glass (-0.0006 \AA/GPa), $\text{Ge}^{4+}\text{-O}$ in GeO_2 glass (-0.0004 \AA/GPa), $\text{W}^{6+}\text{-O}$ in basaltic glass (-0.0001 \AA/GPa), and $\text{Al}^{3+}\text{-O}$ in $\text{CaAl}_2\text{Si}_2\text{O}_8$ glass (-0.0005 \AA/GPa) exhibit more gradual changes (Prescher et al., 2017; Ozawa et al., 2021; Ghosh and Karki, 2018). These Si^{4+} , Ge^{4+} , W^{6+} , and Al^{3+} are the network forming cations with six-fold coordination at $>\sim 30$ GPa. The gradual decrease in these bond lengths may be a result of the volume reduction by enhanced distortion of coordinated octahedra instead of isostructural compression (Spiekermann et al., 2019).

3.2. Spin Crossover of Iron in Silicate Glasses

Previous studies examined possible spin crossovers of ferrous and ferric iron in silicate glasses under high pressures based on X-ray emission spectroscopy (XES) and Mössbauer spectroscopy (Nomura et al., 2011; Gu et al., 2012; Murakami et al., 2014; Mao et al., 2014; Prescher et al., 2014; Dorfman et al., 2016; Solomatova et al., 2017). The Fe^{2+} -O and Fe^{3+} -O bond lengths obtained by XAFS measurements also show the spin state of ferrous and ferric iron at high pressures.

In [Figure 4c](#), we compare the Fe^{2+} -O and Fe^{3+} -O bond lengths in our glass samples determined by the EXAFS analyses with those in Fe-bearing MgSiO_3 melt at 3000 K obtained by first principles molecular dynamics simulations (Ghosh & Karki, 2020). Although the bond lengths in the latter are longer partly because of thermal expansion, they exhibit similar pressure effects. The behavior of the Fe^{2+} -O bond length below 15 GPa is an exception; while it increased rapidly in the Fe-bearing MgSiO_3 melt, it changed little in our reduced glass. Such difference can be attributed to the difference in the coordination number of ferrous iron at ambient pressure; it was shown to be less than four in silicate (basaltic) melts by previous first principles simulations (Bajgain et al., 2015; Solomatova & Caracas, 2019; Ghosh & Karki, 2020), whereas it has been reported to be about five in glasses and melts by experimental studies including the present one (Alderman et al., 2017).

Upon compression from 15 to 83 GPa, the Fe^{2+} -O bond length in our basaltic glass decreased smoothly by ~ 0.1 Å ([Figure 4c](#)). Such shortening is similar to that calculated for the high-spin Fe^{2+} in $\text{Mg}_{0.75}\text{Fe}_{0.25}\text{SiO}_3$ melt (Ghosh & Karki, 2020). They also calculated for the low-spin Fe^{2+} , demonstrating much shorter bond lengths by ~ 0.2 Å

above 15 GPa (such difference is consistent with the difference in the ionic radius between six-fold high-spin and low-spin ferrous iron at 1 bar). The supposed low-spin Fe^{2+} -O bond length in a basaltic glass based on the calculations by Ghosh & Karki (2020) is substantially shorter than that of Fe^{2+} -O observed in this study.

Previous XES measurements of $\text{Mg}_{0.95}\text{Fe}_{0.05}\text{SiO}_3$ glass (Nomura et al., 2011) and $\text{Mg}_{0.8}\text{Fe}_{0.2}\text{SiO}_3$ and $\text{Mg}_{0.75}\text{Fe}_{0.20}\text{Al}_{0.05}\text{SiO}_3$ glasses (Gu et al., 2012) demonstrated a complete spin crossover of ferrous iron at 77 GPa and a partial loss of spin moment at >93 GPa, respectively. In addition, the Mössbauer measurements by Murakami et al. (2014) suggested a transition of Fe^{2+} to an intermediate-spin state in $(\text{Mg}_{0.8}\text{Fe}_{0.2})\text{SiO}_3$ glass. In contrast, Mao et al. (2014) analyzed the XES spectra taking the broadening effect into consideration and argued that all Fe remains in the high-spin state in an (Al, Fe)-bearing silicate glass up to 126 GPa. The Mössbauer study by Solomatova et al. (2017) argued that ferrous iron remains high-spin to ~100 GPa in a basaltic glass. The present data supports high-spin Fe^{2+} in basaltic glasses up to 83 GPa (Figure 4c). The apparent discrepancies among these studies may be attributed to the differences in glass composition.

The compression behavior of the Fe^{3+} -O bond length in our oxidized glass is similar to that theoretically calculated for the high-spin Fe^{3+} in $\text{Mg}_{0.875}\text{Fe}^{3+}_{0.25}\text{Si}_{0.875}\text{O}_3$ melt (Ghosh & Karki, 2020) (Figure 4c). Such similarity supports that Fe^{3+} remains high spin, at least to 60 GPa. The XES and Mössbauer measurements on $\text{Fe}_3\text{Al}_2\text{Si}_3\text{O}_{12}$ almandine glass by Dorfman et al. (2016) argued for the high-spin to low-spin crossover of Fe^{3+} between ambient pressure and 30 GPa. Such discrepancy may be also due to the difference in glass sample composition. Alternatively it is also possible that the Mössbauer observations by

Dorfman and others may be explained by the distortion of coordination polyhedron as argued for an Fe^{3+} -rich sodium silicate glass (Prescher et al., 2014).

3.3. Disproportionation of Fe^{2+} in a Deep Magma Ocean

The earlier experiments performed by Armstrong et al. (2019) observed that the $\text{Fe}^{3+}/\Sigma\text{Fe}$ ratio in a silicate melt increased with increasing pressure above 10 GPa under a given oxygen fugacity buffer, suggesting that Fe^{2+} disproportionates into Fe^{3+} and metal in a deep magma ocean. They attributed it to the smaller partial molar volume of $\text{FeO}_{1.5}$ than that of FeO in melt above 10 GPa. Indeed, the present study indicates that the coordination number of Fe^{3+} increases rapidly from four at 1 atm to six at ~15 GPa (Figure 2). It causes a remarkable reduction in the partial molar volume V of $\text{FeO}_{1.5}$ compared to that of FeO in this pressure range. These support negative $\Delta V (= V_{\text{FeO}_{1.5}} - V_{\text{FeO}})$ and resulting the disproportionation of Fe^{2+} in the magma ocean above 10 GPa (Armstrong et al., 2019). The recent first principles study by Deng et al. (2020) reported the positive ΔV even above 10 GPa, but it is likely due to an underestimation of the coordination number of Fe^{2+} at ambient pressure, which leads to an overestimation of the compressibility of the partial molar volume of FeO .

With increasing pressure above ~15 GPa, the Fe^{2+} -O bond length changed similarly to that of Fe^{3+} -O (Figure 4c). This means that ΔV is almost unchanged upon compression in this pressure range, at least to 60 GPa. If ΔV is negative at 10–25 GPa (Armstrong et al., 2019), it stays negative and expands the stability of Fe^{3+} relative to Fe^{2+} in silicate melts at higher pressures. It therefore supports that the disproportionation of FeO into $\text{Fe}_{1.5}\text{O}$ and metal Fe in a magma ocean is more enhanced with increasing pressure above 10 GPa to lower-mantle conditions. Metal Fe produced by such disproportionation reaction may

have been segregated into the Earth's core, increasing the oxygen fugacity of the magma ocean, which changed the metal-silicate partitioning of siderophile elements (Wade & Wood, 2005) and the composition of early Earth atmosphere (Hirschmann, 2012).

4. Conclusions

Present *in-situ* high-pressure XAFS measurements elucidated the compression behavior of the coordination environments around Fe^{2+} and Fe^{3+} in basaltic glasses up to 83 GPa and 60 GPa, respectively. Pre-edge and EXAFS analyses demonstrated that between 1 atm and ~15 GPa, the coordination number of Fe^{2+} increased from ~5 to 6, while that of Fe^{3+} augmented from almost 4 to 6. At higher pressures, both Fe^{2+} -O and Fe^{3+} -O bond lengths decreased smoothly with increasing pressure, indicating minimal increase in their coordination number. In this pressure range, the observed compression behaviors of the Fe^{2+} -O and Fe^{3+} -O bonds are similar to those of earlier theoretical predictions of high-spin Fe^{2+} and Fe^{3+} in $\text{Mg}_{0.75}\text{Fe}^{2+}_{0.25}\text{SiO}_3$ and $\text{Mg}_{0.875}\text{Fe}^{3+}_{0.25}\text{Si}_{0.875}\text{O}_3$ melts, respectively, suggesting both Fe^{2+} and Fe^{3+} in the basaltic glasses remain high-spin at least to the maximum pressures explored here.

A larger change in the coordination number of Fe^{3+} than that of Fe^{2+} below 15 GPa suggests that the partial molar volume of $\text{FeO}_{1.5}$ is more compressible than that of FeO in this pressure range. It will lead to negative $\Delta V (= V_{\text{FeO}_{1.5}} - V_{\text{FeO}})$ above 10 GPa (Armstrong et al., 2019), which drives the disproportionation of Fe^{2+} into Fe^{3+} and metal Fe in a deep magma ocean. Our data showed that the both the Fe^{2+} -O and Fe^{3+} -O bond lengths decreased similarly with increasing pressure above 15 GPa. It suggests that ΔV would remain negative upon compression at least to 60 GPa, which accelerates the disproportionation reaction at deeper level of the magma ocean.

Open Research

Datasets for this research are found in Tables S1 and S2 available online (from <https://doi.org/10.5281/zenodo.5749615>).

Acknowledgments

K. Yonemitsu is acknowledged for her help in EPMA analyses. This work was supported by the JSPS grants 21H04968 and 20J21667. XAFS measurements was performed with the approval of the Photon Factory (proposal no. 2018S1-001 and 2020G670).

References

- Alderman, O. L. G., Wilding, M. C., Tamalonis, A., Sendelbach, S., Heald, S. M., Benmore, C. J., Johnson, C. E., Johnson, J. A., Hah, H.-Y., & Weber, J. K. R. (2017). Iron K-edge X-ray absorption near-edge structure spectroscopy of aerodynamically levitated silicate melts and glasses. *Chemical Geology*, 453, 169–185. <https://doi.org/10.1016/j.chemgeo.2017.01.020>
- Armstrong, K., Frost, D. J., McCammon, C. A., Rubie, D. C., & Ballaran, T. B. (2019). Deep magma ocean formation set the oxidation state of Earth's mantle. *Science*, 365, 903–906. <https://doi.org/10.1126/science.aax8376>
- Badro, J., Fiquet, G., Guyot, F., Rueff, J. P., Struzhkin, V. V., Vankó, G., & Monaco, G. (2003). Iron partitioning in Earth's mantle: toward a deep lower mantle discontinuity. *Science*, 300, 789–791. <https://doi.org/10.1126/science.1081311>
- Bajgain, S., Ghosh, D. B., & Karki, B. B. (2015). Structure and density of basaltic melts at mantle conditions from first-principles simulations. *Nature communications*, 6, 8578. <https://doi.org/10.1038/ncomms9578>

318 Berry, A. J., O'Neill, H. S. C., Jayasuriya, K. D., Campbell, S. J., & Foran, G. J. (2003).
 319 XANES calibrations for the oxidation state of iron in a silicate glass. *American*
 320 *Mineralogist*, 88, 967–977. <https://doi.org/10.2138/am-2003-0704>
 321 Boubnov, A., Lichtenberg, H., Mangold, S., & Grunwaldt, J. D. (2015). Identification of
 322 the iron oxidation state and coordination geometry in iron oxide-and zeolite-based
 323 catalysts using pre-edge XAS analysis. *Journal of Synchrotron Radiation*, 22, 410–
 324 426. <https://doi.org/10.1107/S1600577514025880>
 325 Deng, J., Du, Z., Karki, B. B., Ghosh, D. B., & Lee, K. K. (2020). A magma ocean origin
 326 to divergent redox evolutions of rocky planetary bodies and early atmospheres.
 327 *Nature communications*, 11, 2007. <https://doi.org/10.1038/s41467-020-15757-0>
 328 Dorfman, S. M., Dutton, S. E., Potapkin, V., Chumakov, A. I., Rueff, J. P., Chow, P.,
 329 Xiao, Y., Cava, R. J., Duffy, T. S., McCammon, C. A., & Gillet, P. (2016). Electronic
 330 transitions of iron in almandine-composition glass to 91 GPa. *American Mineralogist*,
 331 101, 1659–1667. <https://doi.org/10.2138/am-2016-5606>
 332 Farges, F., Lefrère, Y., Rossano, S., Berthereau, A., Calas, G., & Brown Jr, G. E. (2004).
 333 The effect of redox state on the local structural environment of iron in silicate glasses:
 334 A combined XAFS spectroscopy, molecular dynamics, and bond valence
 335 study. *Journal of Non-Crystalline Solids*, 344, 176–188.
 336 <https://doi.org/10.1016/j.jnoncrysol.2004.07.050>
 337 Ghosh, D. B., & Karki, B. B. (2018). First-principles molecular dynamics simulations of
 338 anorthite (CaAl₂Si₂O₈) glass at high pressure. *Physics and Chemistry of Minerals*, 45,
 339 575–587. <https://doi.org/10.1007/s00269-018-0943-4>

- Ghosh, D. B., & Karki, B. B. (2020). Effects of valence and spin of Fe in MgSiO₃ melts: structural insights from first-principles molecular dynamics simulations. *Geochimica et Cosmochimica Acta*, 279, 107–118. <https://doi.org/10.1016/j.gca.2020.03.040>
- Giuli, G., Alonso-Mori, R., Cicconi, M. R., Paris, E., Glatzel, P., Eeckhout, S. G., & Scaillet, B. (2012). Effect of alkalis on the Fe oxidation state and local environment in peralkaline rhyolitic glasses. *American Mineralogist*, 97, 468–475. <https://doi.org/10.2138/am.2012.3888>
- Gu, C., Catalli, K., Grocholski, B., Gao, L., Alp, E., Chow, P., Xiao, Y., Cynn, H., Evans, W. J., & Shim, S. H. (2012). Electronic structure of iron in magnesium silicate glasses at high pressure. *Geophysical Research Letters*, 39. <https://doi.org/10.1029/2012GL053950>
- Hirschmann, M. M. (2012). Magma ocean influence on early atmosphere mass and composition. *Earth and Planetary Science Letters*, 341–344, 48–57. <https://doi.org/10.1016/j.epsl.2012.06.015>
- Hong, X., Newville, M., Duffy, T. S., Sutton, S. R., & Rivers, M. L. (2014). X-ray absorption spectroscopy of GeO₂ glass to 64 GPa. *Journal of Physics: Condensed Matter*, 26, 035104. <https://doi.org/10.1088/0953-8984/26/3/035104>
- Karki, B. B., Ghosh, D. B., Maharjan, C., Karato, S. I., & Park, J. (2018). Density-pressure profiles of Fe-bearing MgSiO₃ liquid: effects of valence and spin states, and implications for the chemical evolution of the lower mantle. *Geophysical Research Letters*, 45, 3959–3966. <https://doi.org/10.1029/2018GL077149>
- Kress, V. C., & Carmichael, I. S. E. (1991). The compressibility of silicate liquids containing Fe₂O₃ and the effect of composition, temperature, oxygen fugacity and

pressure on their redox states. *Contributions to Mineralogy and Petrology*, 108, 82–92. <https://doi.org/10.1007/BF00307328>

Lange, R. A., & Carmichael, I. S. E. (1987). Densities of Na₂O-K₂O-CaO-MgO-FeO-Fe₂O₃-Al₂O₃-TiO₂-SiO₂ liquids: new measurements and derived partial molar properties. *Geochimica et Cosmochimica Acta*, 51, 2931–2946. [https://doi.org/10.1016/0016-7037\(87\)90368-1](https://doi.org/10.1016/0016-7037(87)90368-1)

Mao, Z., Lin, J. F., Yang, J., Wu, J., Watson, H. C., Xiao, Y., Chow, P., & Zhao, J. (2014). Spin and valence states of iron in Al-bearing silicate glass at high pressures studied by synchrotron Mössbauer and X-ray emission spectroscopy. *American Mineralogist*, 99, 415–423. <https://doi.org/10.2138/am.2014.4490>

Murakami, M., Goncharov, A. F., Hirao, N., Masuda, R., Mitsui, T., Thomas, S. M., & Bina, C. R. (2014). High-pressure radiative conductivity of dense silicate glasses with potential implications for dark magmas. *Nature communications*, 5, 5428. <https://doi.org/10.1038/ncomms6428>

Nomura, R., Ozawa, H., Tateno, S., Hirose, K., Hernlund, J., Muto, S., Ishii, H., & Hiraoka, N. (2011). Spin crossover and iron-rich silicate melt in the Earth's deep mantle. *Nature*, 473, 199–202. <https://doi.org/10.1038/nature09940>

O'Neill, H. S. C., Berry, A. J., McCammon, C. C., Jayasuriya, K. D., Campbell, S. J., & Foran, G. (2006). An experimental determination of the effect of pressure on the Fe³⁺/ΣFe ratio of an anhydrous silicate melt to 3.0 GPa. *American Mineralogist*, 91, 404–412. <https://doi.org/10.2138/am.2005.1929>

Ozawa, K., Hirose, K., Kuwayama, Y., & Takahashi, Y. (2021). The pressure-induced local structural change around tungsten in silicate glass. *Geochemical Perspectives Letters*, 18. <https://doi.org/10.7185/geochemlet.2116>

387 Prescher, C., Weigel, C., McCammon, C., Narygina, O., Potapkin, V., Kuppenko, I.,
 388 Sinmyo, R., Chumakov, A. I., & Dubrovinsky, L. (2014). Iron spin state in silicate
 389 glass at high pressure: implications for melts in the Earth's lower mantle. *Earth and*
 390 *Planetary Science Letters*, 385, 130–136. <https://doi.org/10.1016/j.epsl.2013.10.040>
 391 Prescher, C., Prakapenka, V. B., Stefanski, J., Jahn, S., Skinner, L. B., & Wang, Y. (2017).
 392 Beyond sixfold coordinated Si in SiO₂ glass at ultrahigh pressures. *Proceedings of the*
 393 *National Academy of Sciences USA*, 114, 10041–10046.
 394 <https://doi.org/10.1073/pnas.1708882114>
 395 Sanloup, C., Drewitt, J., Konôpková, Z., Dalladay-Simpson, P., Morton, D. M., Rai, N.,
 396 Van Westrenen, W., & Morgenroth, W. (2013a). Structural change in molten basalt
 397 at deep mantle conditions. *Nature*, 503, 104–107.
 398 <https://doi.org/10.1038/nature12668>
 399 Sanloup, C., Drewitt, J. W. E., Crépeisson, C., Kono, Y., Park, C., McCammon, C., Hennet,
 400 L., Brassamin, S., & Bychkov, A. (2013b). Structure and density of molten fayalite
 401 at high pressure. *Geochimica et Cosmochimica Acta*, 118, 118–128.
 402 <https://doi.org/10.1016/j.gca.2013.05.012>
 403 Solomatova, N. V., Jackson, J. M., Sturhahn, W., Rossman, G. R., & Roskosz, M. (2017).
 404 Electronic environments of ferrous iron in rhyolitic and basaltic glasses at high
 405 pressure. *Journal of Geophysical Research: Solid Earth*, 122, 6306–6322.
 406 <https://doi.org/10.1002/2017JB014363>
 407 Solomatova, N. V., & Caracas, R. (2019). Pressure-induced coordination changes in a
 408 pyrolitic silicate melt from ab initio molecular dynamics simulations. *Journal of*
 409 *Geophysical Research: Solid Earth*, 124, 11232–11250.
 410 <https://doi.org/10.1029/2019JB018238>

- Spiekermann, G., Harder, M., Gilmore, K., Zalden, P., Sahle, C. J., Petitgirard, S., Wilke, M., Biedermann, N., Weis, C., Morgenroth, W., Tse, J. S., Kulik, E., Nishiyama, N., Yavas, H., & Sternemann, C. (2019). Persistent octahedral coordination in Amorphous GeO₂ up to 100 GPa by K β'' X-Ray emission spectroscopy. *Physical Review X*, 9, 011025. <https://doi.org/10.1103/PhysRevX.9.011025>
- Wade, J., & Wood, B. J. (2005). Core formation and the oxidation state of the Earth. *Earth and Planetary Science Letters*, 236, 78–95. <https://doi.org/10.1016/j.epsl.2005.05.017>
- Waychunas, G. A., Apter, M. J., & Brown Jr., G. E. (1983). X-ray K-edge absorption spectra of Fe minerals and model compounds: near-edge structure. *Physics and Chemistry of Minerals*, 10, 1–9. <https://doi.org/10.1007/BF01204319>
- Wilke, M., Farges, F., Petit, P. E., Brown Jr., G. E., & Martin, F. (2001). Oxidation state and coordination of Fe in minerals: an Fe K-XANES spectroscopic study. *American Mineralogist*, 86, 714–730. <https://doi.org/10.2138/am-2001-5-612>
- Wilke, M., Partzsch, G. M., Bernhardt, R., & Lattard, D. (2005). Determination of the iron oxidation state in basaltic glasses using XANES at the K-edge. *Chemical Geology*, 220, 143–161. <https://doi.org/10.1016/j.chemgeo.2005.03.004>
- Wilke, M., Farges, F., Partzsch, G. M., Schmidt, C., & Behrens, H. (2007). Speciation of Fe in silicate glasses and melts by in-situ XANES spectroscopy. *American Mineralogist*, 92, 44–56. <https://doi.org/10.2138/am.2007.1976>
- Zhang, F., & Oganov, A. R. (2006). Valence state and spin transitions of iron in Earth's mantle silicates. *Earth and Planetary Science Letters*, 249, 436–443. <https://doi.org/10.1016/j.epsl.2006.07.023>

Zhang, H. L., Hirschmann, M. M., Cottrell, E., & Withers, A. C. (2017). Effect of pressure on $\text{Fe}^{3+}/\Sigma\text{Fe}$ ratio in a mafic magma and consequences for magma ocean redox gradients. *Geochimica et Cosmochimica Acta*, 204, 83–103.
<https://doi.org/10.1016/j.gca.2017.01.023>

References from the supporting information

Akahama, Y., & Kawamura, H. (2004). High-pressure Raman spectroscopy of diamond anvils to 250 GPa: Method for pressure determination in the multimegabar pressure range. *Journal of Applied Physics*, 96, 3748–3751. <https://doi.org/10.1063/1.1778482>

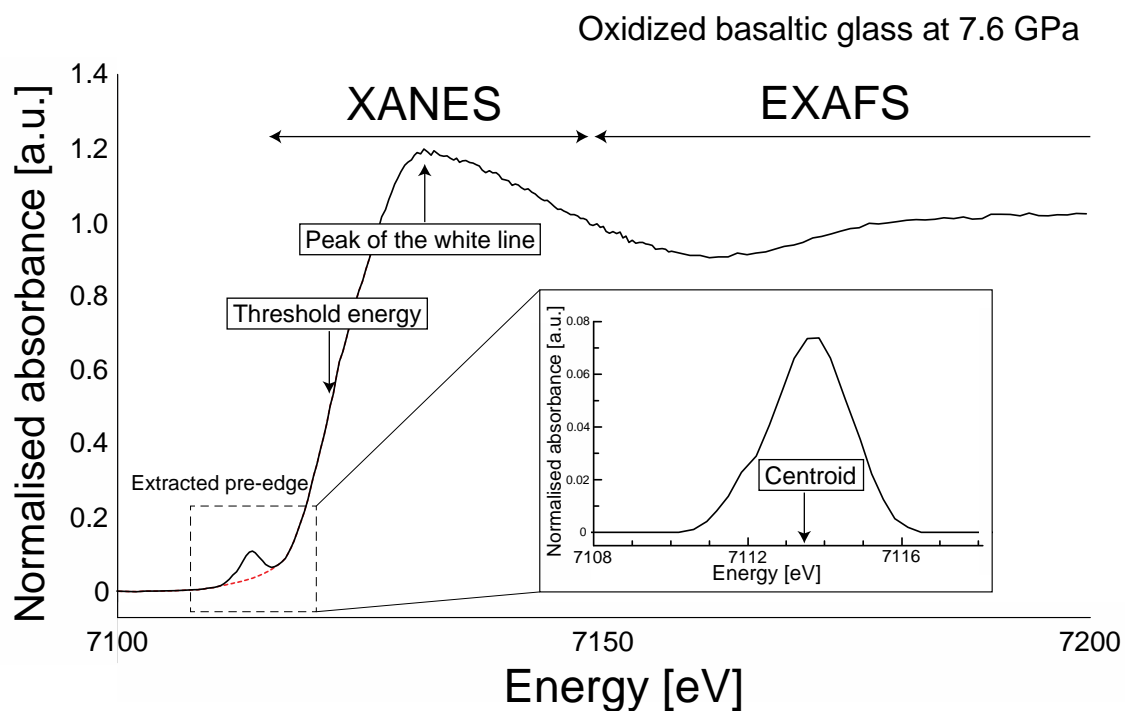
Berry, A. J., Stewart, G. A., O'Neill, H. S. C., Mallmann, G., & Mosselmans, J. F. W. (2018). A re-assessment of the oxidation state of iron in MORB glasses. *Earth and Planetary Science Letters*, 483, 114–123. <https://doi.org/10.1016/j.epsl.2017.11.032>

Mao, H. K., Bell, P. M., Shaner, J. T., & Steinberg, D. J. (1978). Specific volume measurements of Cu, Mo, Pd, and Ag and calibration of the ruby R_1 fluorescence pressure gauge from 0.06 to 1 Mbar. *Journal of Applied Physics*, 49, 3276–3283. <https://doi.org/10.1063/1.325277>

Merkel, S., & Yagi, T. (2005). X-ray transparent gasket for diamond anvil cell high pressure experiments. *Review of Scientific Instruments*, 76, 046109. <https://doi.org/10.1063/1.1884195>

Zabinsky, S. I., Rehr, J. J., Ankudinov, A., Albers, R. C., & Eller, M. J. (1995). Multiple-scattering calculations of X-ray-absorption spectra. *Physical Review B*, 52, 2995. <https://doi.org/10.1103/PhysRevB.52.2995>

455

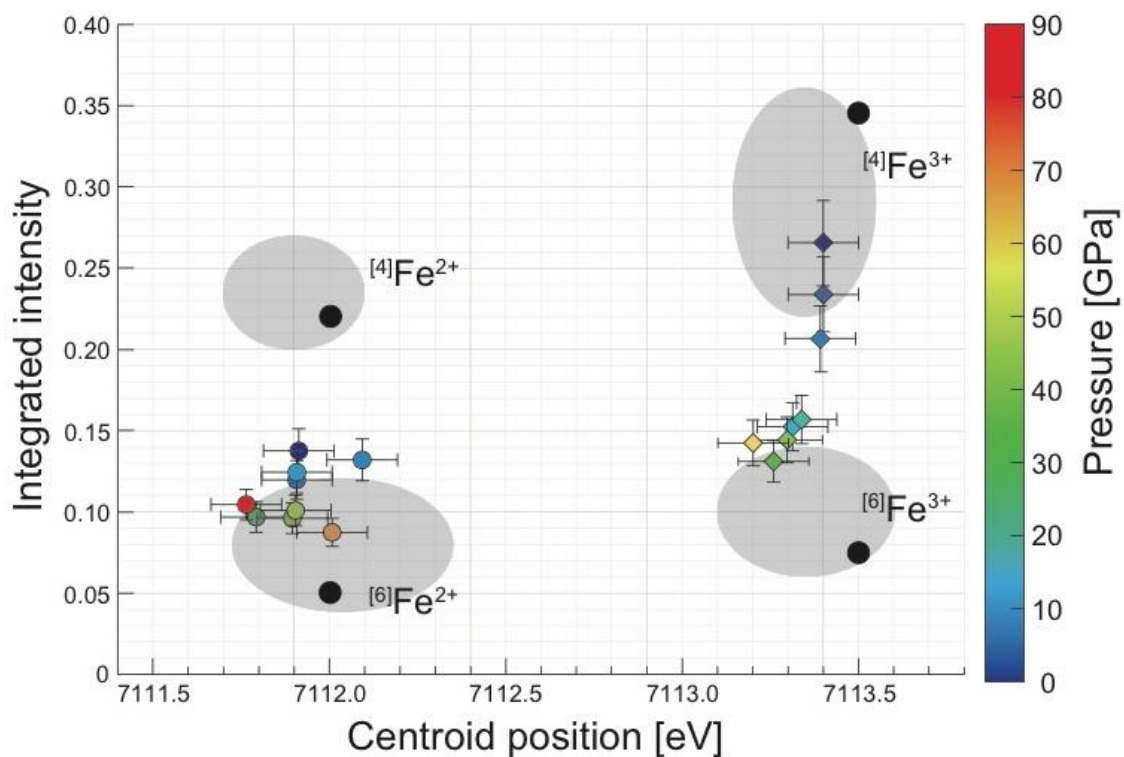


456

457 **Figure 1.** The μ -XAFS spectrum of oxidized basaltic glass in a DAC collected at 7.6 GPa,
 458 including the pre-edge features with centroid position, XANES with the threshold energy
 459 and the peak of the while line, and EXAFS oscillations. Red dashed line is a cubic spline
 460 function for the background of the pre-edge signals (Wilke et al., 2001).

461

462

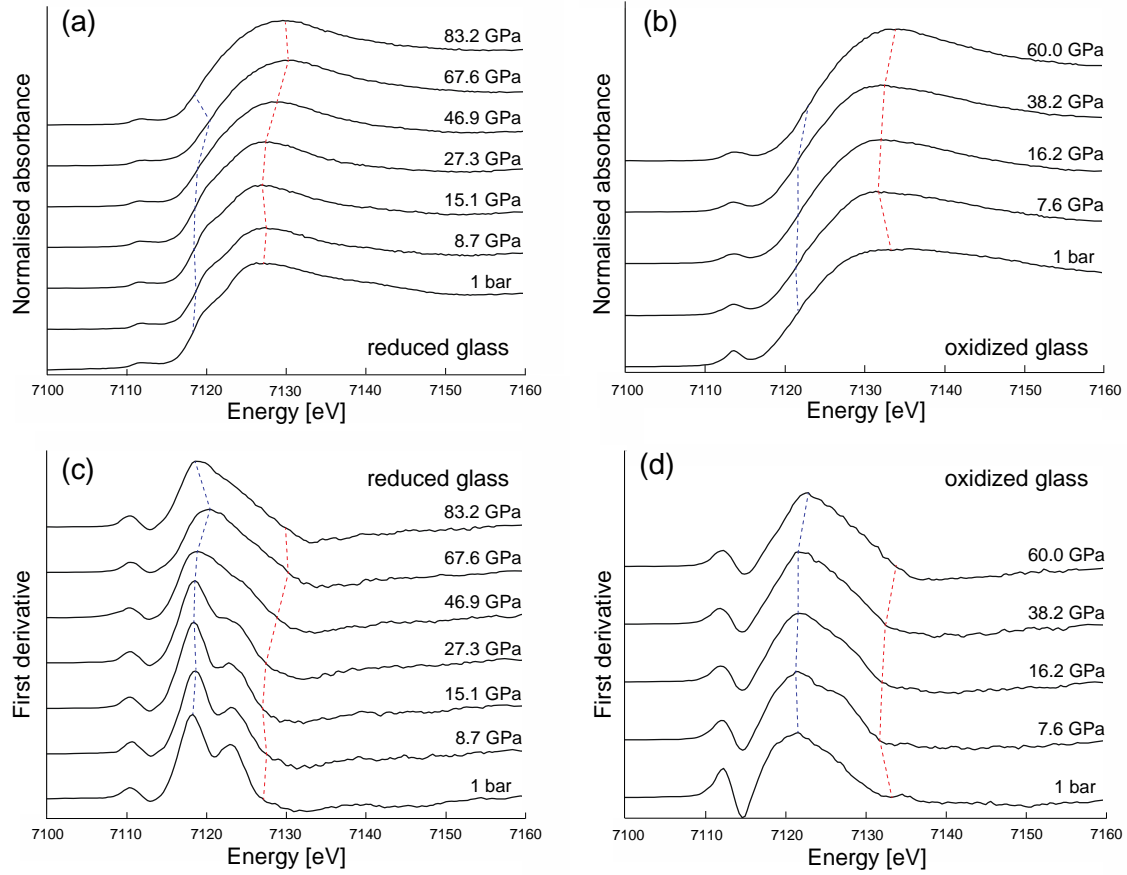


463

464 **Figure 2.** The pre-edge variogram of the centroid position vs. integrated intensity for
 465 reduced (circles) and oxidized basaltic glasses (diamonds) at high pressures. Pressure is
 466 given by color. Shaded areas indicate the ranges for ferrous and ferric iron with four- and
 467 six-fold coordination (Boubnov et al., 2015). Black circles represent the data for minerals
 468 with 4- and 6-fold ferrous/ferric iron given by Wilke et al. (2001).

469

470



471

Figure 3. Fe K-edge XANES spectra and their first derivative spectra obtained by three-point moving average for reduced (a, c) and oxidized (b, d) basaltic glasses at high pressures. The spectrum of the reduced glass at 67.6 GPa is of a W-doped basaltic glass used in Ozawa et al. (2021). Red and blue dashed lines indicate pressure-evolutions of the peak energy of the white line and the threshold energy, respectively (see Figure 1).

477

F

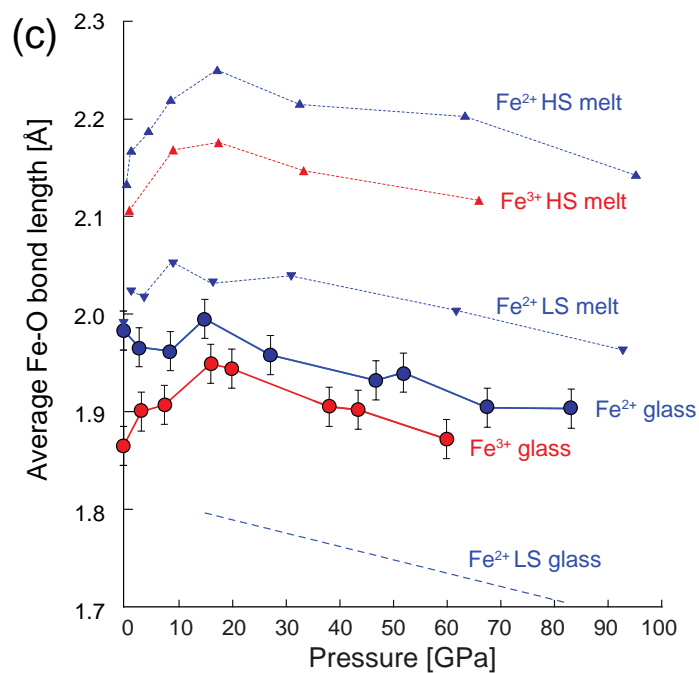
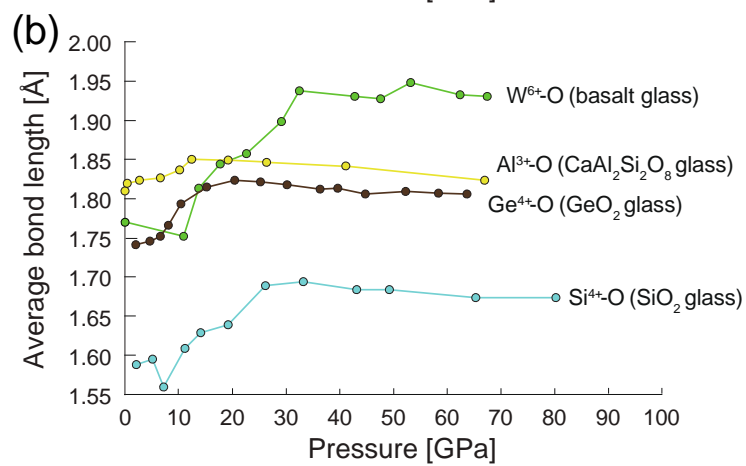
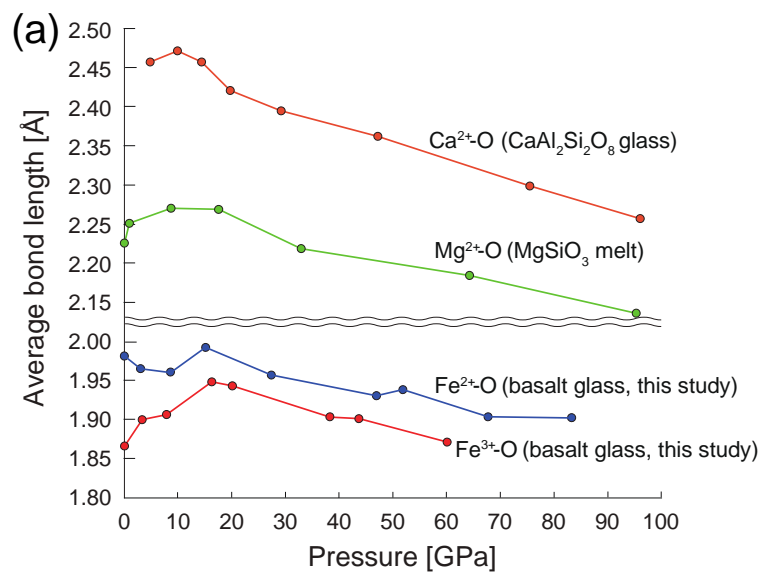


Figure 4. (a, b) Interatomic distances between various cations and oxygen in silicate/germanate melt and glasses; Ca^{2+} -O and Al^{3+} -O (Ghosh & Karki, 2018), Mg^{2+} -O (Ghosh & Karki, 2020), $\text{Fe}^{2+/3+}$ -O (this study), Si^{4+} -O (Prescher et al., 2017), Ge^{4+} -O (Hong et al., 2014), and W^{6+} -O (Ozawa et al., 2021). (c) Comparison of the Fe^{2+} -O (blue lines) and Fe^{3+} -O (red lines) bond lengths in our basaltic glasses with those in Fe-bearing MgSiO_3 melts (dotted lines) at 3000 K obtained by ab initio molecular dynamics simulations (Ghosh & Karki, 2020). The blue dashed line is for low-spin Fe^{2+} in the glass, estimated from a difference in the calculated Fe^{2+} -O bond length between high-spin and low-spin states.



Geophysical Research Letters

Supporting Information for

**High-Pressure XAFS Measurements of the Coordination Environments of Fe²⁺ and Fe³⁺
in Basaltic Glasses**

Keisuke Ozawa¹, Kei Hirose^{1,2}, and Yoshio Takahashi^{1,3}

¹Department of Earth and Planetary Science, The University of Tokyo, Tokyo, Japan

²Earth-Life Science Institute, Tokyo Institute of Technology, Tokyo, Japan

³Institute of Materials Structure Science, High-Energy Accelerator Research Organization, Tsukuba, Ibaraki, Japan

Contents of this file

Experimental Methods

Figures S1–S3

Tables S1, S2

Experimental Methods

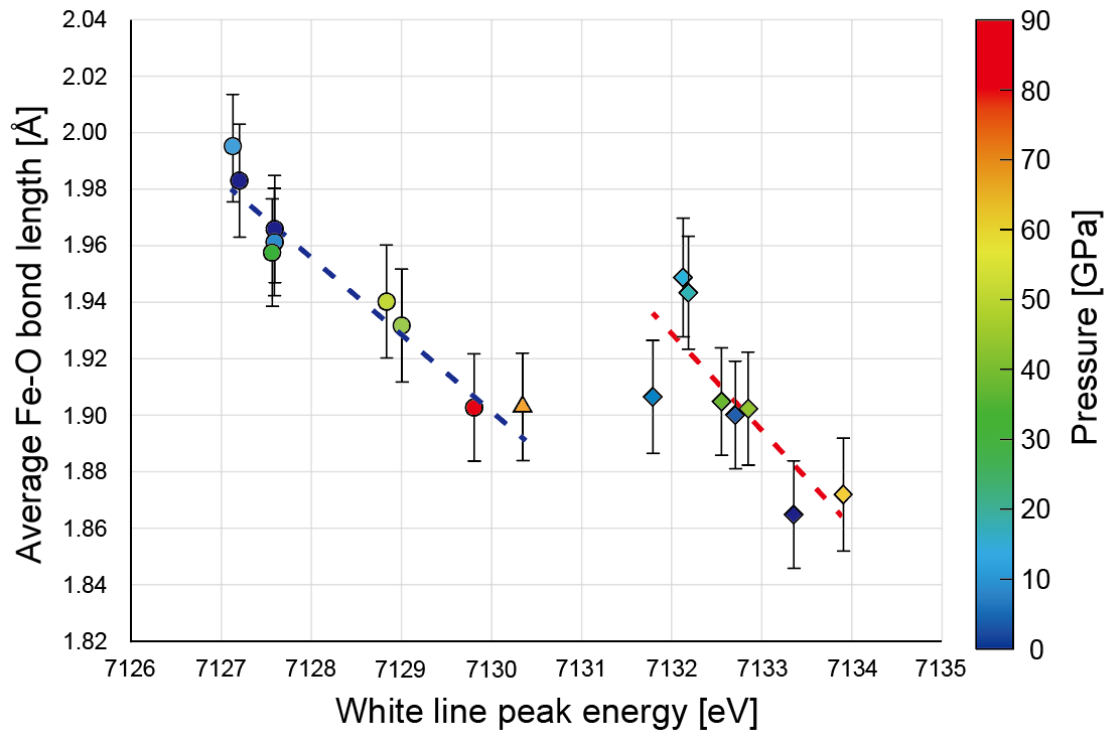
A couple of basaltic glasses were synthesized under reduced and oxidized conditions for the present XAFS measurements. Their chemical compositions and homogeneity were examined with an electron probe microanalyzer (FE-EPMA, JEOL JXA-8530F) (Table S1). They were prepared originally from gel and melted in reducing $\text{H}_2\text{-CO}_2$ gas atmosphere at 1473 K (three log units below the QFM buffer) and in air (oxidizing condition) at 1573 K, respectively, for 30 mins. Under the former reducing condition, ferrous iron should be predominant in the glass ($\text{Fe}^{2+}/\Sigma\text{Fe} = 0.985$) according to Berry et al. (2018). On the other hand, Fe in the latter oxidized glass should be dominated by ferric iron.

We collected both the XANES and EXAFS spectra of these basaltic glasses with increasing pressure at the beamline BL-4A, the Photon Factory, KEK with a beam focused to $5\text{ }\mu\text{m} \times 5\text{ }\mu\text{m}$ area on a sample by using a K-B mirror system (Figure 1). The spectrum of Fe metal foil was also obtained in a similar manner at ambient condition to calibrate the X-ray energy based on the first inflection point of Fe metal foil at 7111.08 eV following Wilke et al. (2001). Basaltic glasses were compressed to high pressures in a diamond-anvil cell (DAC) using flat anvils with 200–600 μm culet size. In order to minimize X-ray absorption, we employed an X-ray transparent gasket (Merkel & Yagi, 2005) and collected the XAFS spectra under the experimental setting same as described in Ozawa et al. (2021). Measurements were performed near the K-edge of Fe in the fluorescence yield mode. Pressure was measured based on a Raman shift of a diamond anvil above 10 GPa (Akahama & Kawamura, 2004) and the ruby fluorescence method at lower pressures (Mao et al., 1978).

The XAFS scan was performed in an energy range of 7065–7450 eV with 0.3 eV steps for the pre-edge and XANES regions and > 0.9 eV steps for other regions. The spectra were normalized by the average absorbance at the 7200–7300 eV region. Then, the pre-edge feature was obtained by subtracting background that is estimated by using a cubic spline function (Wilke et al., 2001) (Figure 1). After the extraction, the centroid position (intensity-weighted pre-edge position) and the intensity of the pre-edge absorption were calculated (Table S2). We considered uncertainties to be $\pm 10\%$ in pre-edge intensity and ± 0.1 eV in the centroid energy following Alderman et al. (2017). The pre-edge intensities at 1 bar for both reduced and oxidized basaltic glasses obtained here in the fluorescence yield mode are comparable to those measured in the transmission mode in Wilke et al. (2005). It indicates that the thickness effect on the pre-edge intensity is negligible compared to the uncertainty in the present measurements.

EXAFS spectra were analyzed by the REX2000 software (Rigaku Co. Ltd.) The k^3 -weighted EXAFS oscillation was extracted from each spectrum, and Fourier transformed within the k -range of 2.6–8.4 \AA^{-1} to the radial structure functions. In order to extract information on the nearest neighbors of Fe atoms from the radial structural function, the first-neighbour shell EXAFS was filtered out using Hanning window function. The filtered radial structural functions were back-transformed to k -space using the backscattering amplitudes, and phase-shift functions of Fe-O were extracted by the FEFF 7.0 (Zabinsky et al., 1995) based on the structure of FeSiO_3 ferrosilite. Curve fitting analysis was performed for the first shell (Fe-O).

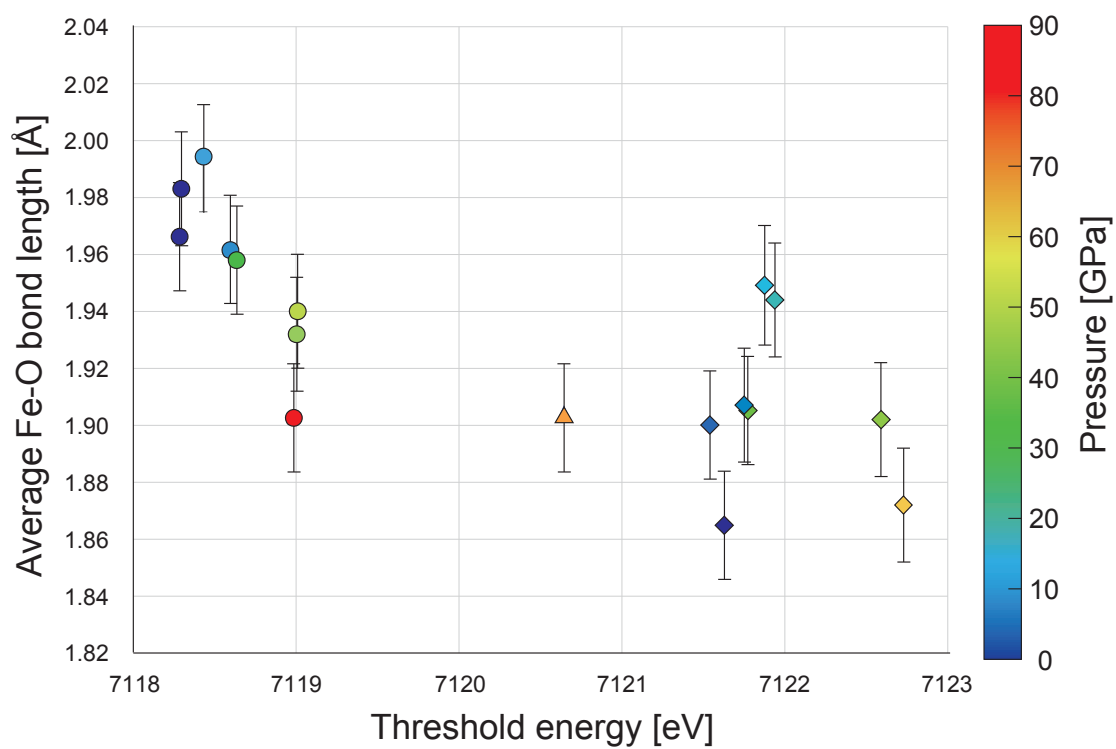
63



64

65 **Figure S1.** The peak energy of the white line vs. the average Fe²⁺-O (circles, reduced
 66 glass; triangle, W-doped glass used in Ozawa et al., 2021) and Fe³⁺-O bond lengths
 67 (diamonds, oxidized glass).
 68

69



70

71 **Figure S2.** The threshold energy vs. the average Fe^{2+} -O and Fe^{3+} -O bond lengths.
 72 Symbols are the same as those in [Figure S1](#).

73

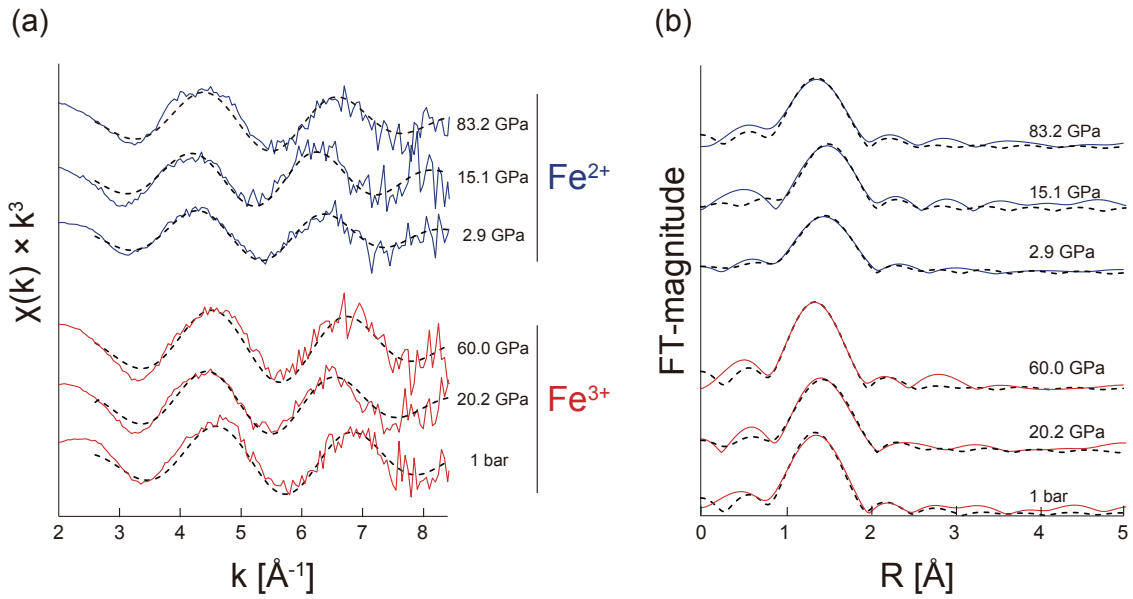


Figure S3. EXAFS oscillations and radial structure functions of Fe in the reduced (blue) and oxidized (red) basaltic glasses. (a) k^3 -weighted oscillations, $\chi(k) \times k^3$, extracted from EXAFS spectra. (b) The radial structural function at the K-edge for Fe which was Fourier transformed (FT) from k^3 -weighted EXAFS oscillations in (a). The black dashed curves in (a) and (b) show simulation data of EXAFS spectra using a parameter extracted by FEFF 7.0.

Table S1

Chemical Compositions of Reduced and Oxidized Basaltic Glasses

wt%	Reduced glass	Oxidized glass
SiO ₂	49.50(35)	50.33(58)
TiO ₂	1.09(5)	1.13(6)
Al ₂ O ₃	14.68(11)	14.77(13)
FeO*	9.53(13)	10.39(12)
MgO	8.42(11)	8.45(9)
CaO	9.52(3)	9.36(11)
Na ₂ O	2.89(16)	3.39(7)
K ₂ O	0.12(2)	0.14(3)
Total	95.76	97.97

The values in parentheses represent one standard deviations in the last digits.

*total Fe as FeO.

Table S2*Pre-edge, XANES, and EXAFS Data for Reduced and Oxidized Basaltic Glasses*

	Pressure (GPa)	Pre-edge		XANES		EXAFS	
		Centroid (eV)	Intensity	Threshold energy (eV)	Peak Energy (eV)	k range	Fe-O bond length (Å)
Reduced glass	1 bar	7111.92	0.1381	7118.30	7127.20	2.6–8.4	1.983 (20)
	2.9	7111.91	0.1200	7118.28	7127.58	2.6–8.4	1.966 (19)
	8.7	7112.09	0.1313	7118.60	7127.59	2.6–8.4	1.962 (19)
	15.1	7111.92	0.1248	7118.43	7127.13	2.6–8.4	1.995 (18)
	27.3	7111.79	0.0970	7118.64	7127.55	2.6–8.4	1.958 (19)
	46.9	7111.89	0.0968	7119.00	7128.99	2.6–8.4	1.932 (20)
	52.0	7111.91	0.1021	7119.01	7128.83	2.6–8.4	1.940 (20)
	67.6*	7112.01	0.0873	7120.64	7130.34	2.6–8.4	1.904 (19)
	83.2	7111.76	0.1044	7118.98	7129.81	2.6–8.4	1.903 (19)
Oxidized glass	1 bar	7113.40	0.2665	7121.63	7133.36	2.6–8.4	1.865 (19)
	3.3	7113.40	0.2332	7121.54	7132.70	2.6–8.4	1.900 (19)
	7.6	7113.39	0.2071	7121.75	7131.79	2.6–8.4	1.907 (20)
	16.2	7113.32	0.1514	7121.88	7132.13	2.6–8.4	1.949 (21)
	20.1	7113.34	0.1578	7121.94	7132.19	2.6–8.4	1.944 (20)
	38.2	7113.26	0.1312	7121.77	7132.56	2.6–8.4	1.905 (19)
	43.6	7113.30	0.1449	7122.59	7132.85	2.6–8.4	1.902 (20)
	60.0	7113.20	0.1420	7122.73	7133.91	2.6–8.4	1.872 (20)

The values in parentheses represent one standard deviations in the last digits. Uncertainties in the pre-edge intensity and the centroid energy are $\pm 10\%$ and ± 0.1 eV, respectively.

*Reduced W-doped glass used in Ozawa et al. (2021).